Electronic Supplementary Material (ESI) for Journal of Materials Chemistry A.

Supporting Information

Table S1 Summary of detail performance parameters of reported PSCs with all-inorganic materials

Perovskites	Device Structures	J_{sc} (mA cm^2)	PCE (%)	Ref
$CsPbIBr_2$	FTO/c-TiO_2/$CsPbIBr_2$/Au	8.7	4.7	S1
$CsPbBr_3$	FTO/c-TiO_2/m- TiO_2/$CsPbBr_3$/Carbon	5.7	5.0	S2
$CsPbBr_3$	FTO/c-TiO_2/m- TiO_2/$CsPbBr_3$/Carbon	7.4	6.7	S3
$CsPbBr_3$	FTO/c-TiO_2/m- TiO_2/$CsPbBr_3$/Carbon	7.46	7.54	S4
$CsPbI_3$	FTO/c-TiO_2/m- TiO_2-Al_2O_3/$CsPbI_3$/Carbon	14.65	5.31	S5
$CsPbI_2Br$	FTO/c-Nb_2O_5/ $CsPbI_2Br$/Carbon	14.02	12.0	S6
$CsPbIBr_2$	FTO/c-TiO_2/$CsPb_{1-x}Mn_xI_{1+2x}Br_{2-2x}$/Carbon	13.15	7.36	S7
$CsPbI_3$	FTO/c-TiO_2/$CsPbI_3$/NiO/Au	5.58	2.0	S8
This work	**FTO/c-TiO_2/$CsPbI_3$/BP/CuSCN/Au**	**19.3**	**14.17**	

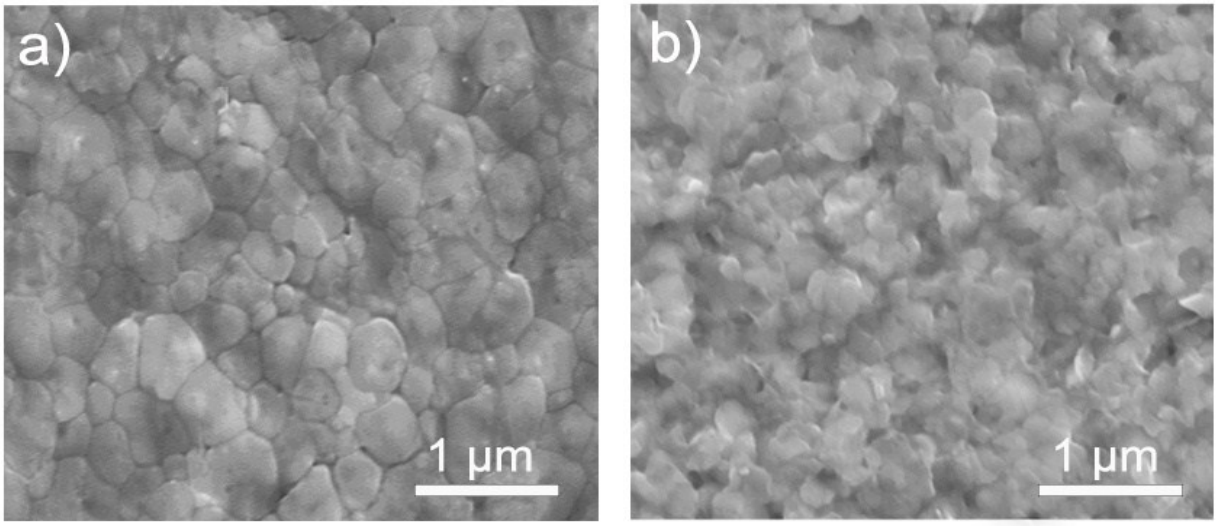

Figure S1 a) SEM image of pristine $CsPbI_3$ film. b) SEM image of $CsPbI_3$-BP film.

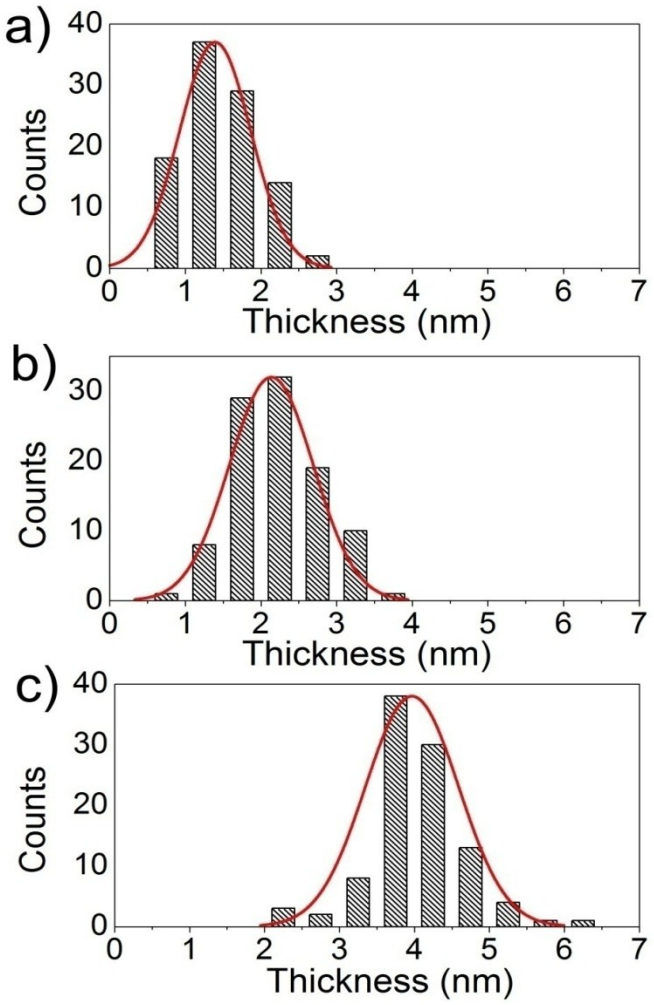

Figure S2 The histogram of thickness distributions of 2D BP samples with different exfoliated conditions.

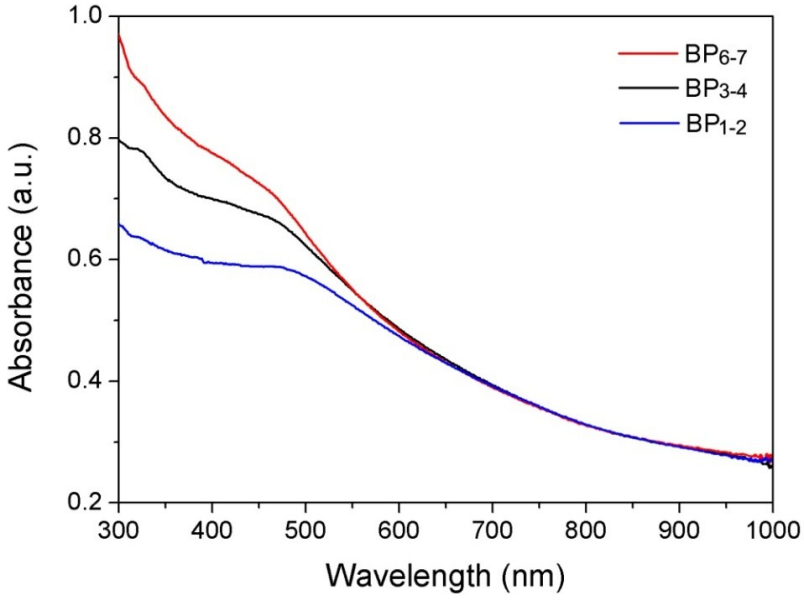

Figure S3 UV-vis-NIR spectra of $BP_{1\text{-}2}$, $BP_{3\text{-}4}$ and $BP_{6\text{-}7}$ film samples

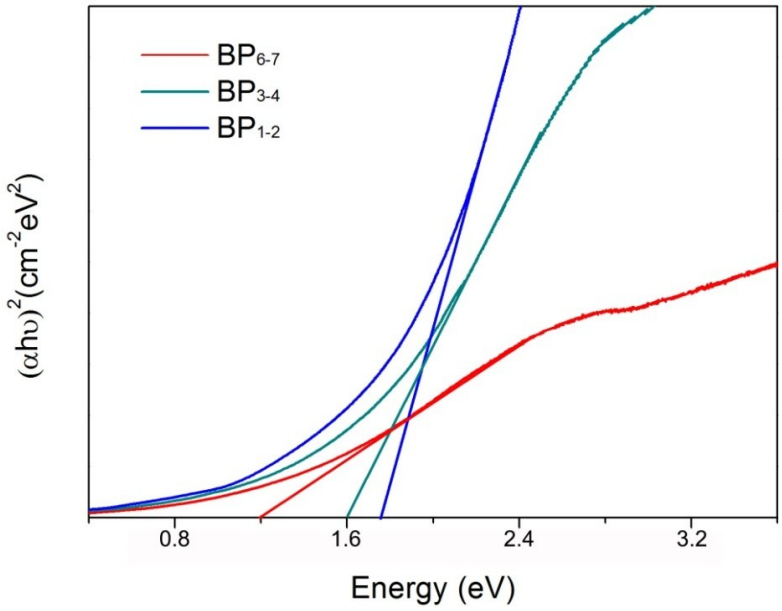

Figure S4 Tauc plots of BP_{1-2}, BP_{3-4} and BP_{6-7} samples calculated from optical absorption spectra.

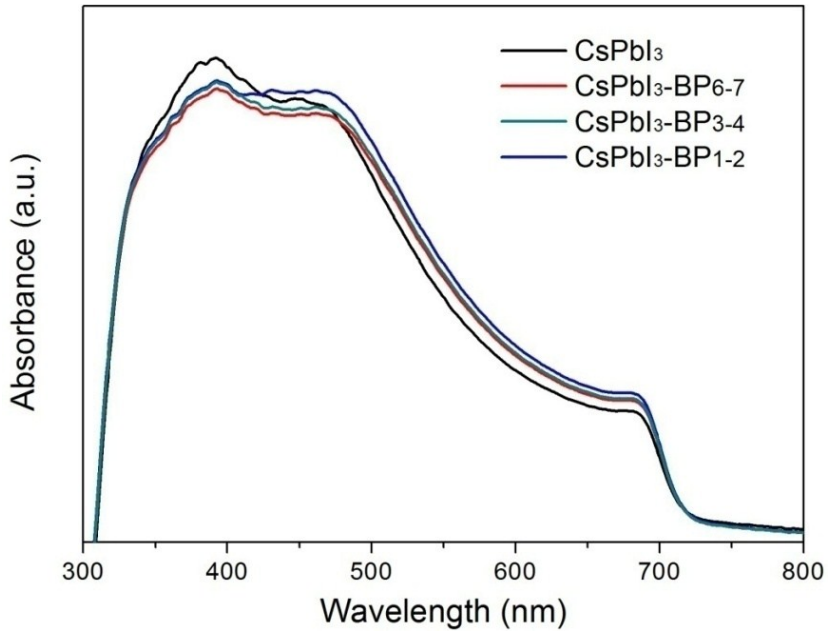

Figure S5 UV-vis spectra of pristine $CsPbI_3$ film and $CsPbI_3$-2D BP films.

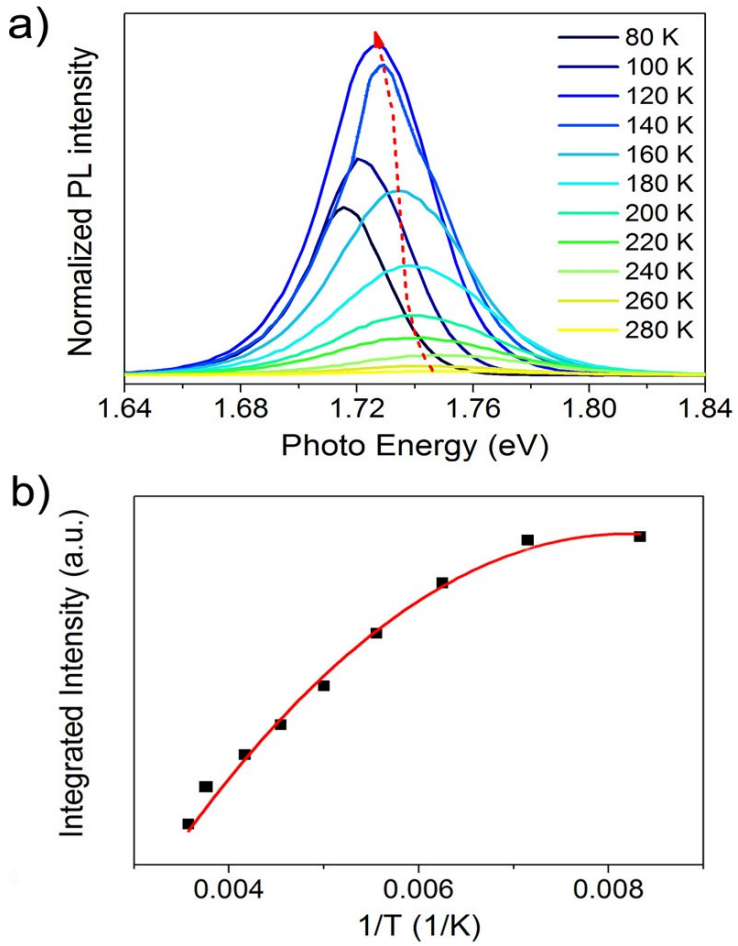

Figure S6 a) Temperature-dependent PL spectra of $CsPbI_3$-CuSCN. b) corresponding Temperature dependent date of the integrated PL intensity of $CsPbI_3$-CuSCN.

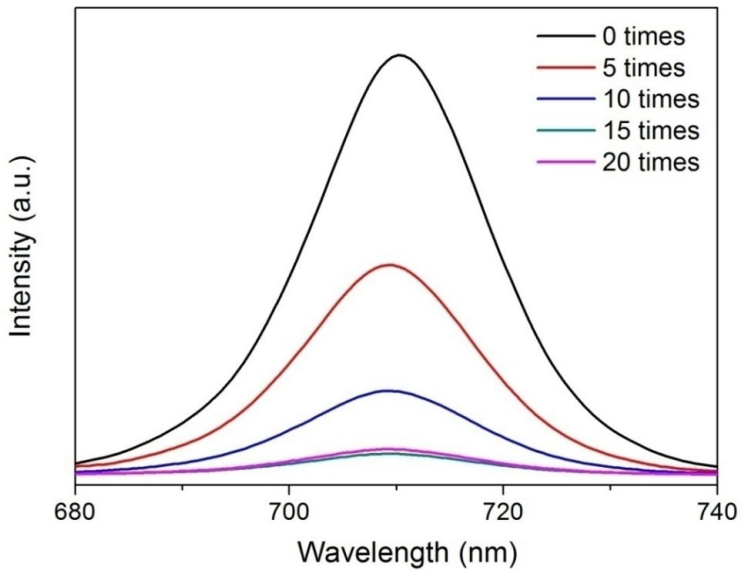

Figure S7 PL spectra of $CsPbI_3$-2D BP films with different deposition times of BPs.

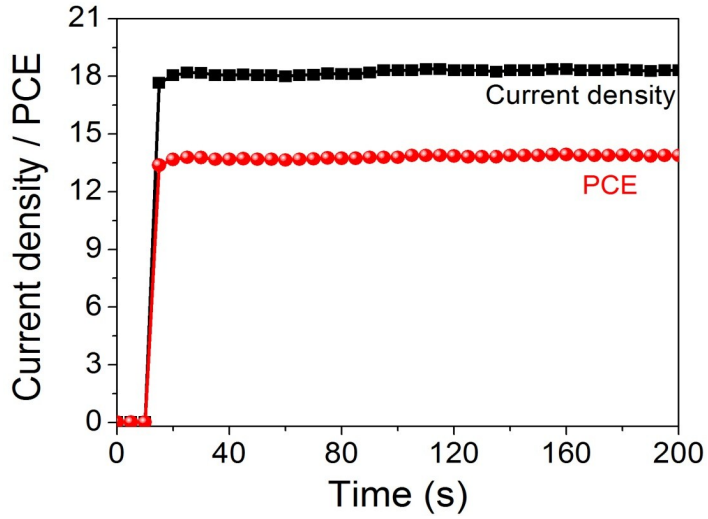

Figure S8 Stabilized photocurrent and efficiency measurement of the best device for $CsPbI_3$-$BP_{1\text{-}2}$ heterostructure.

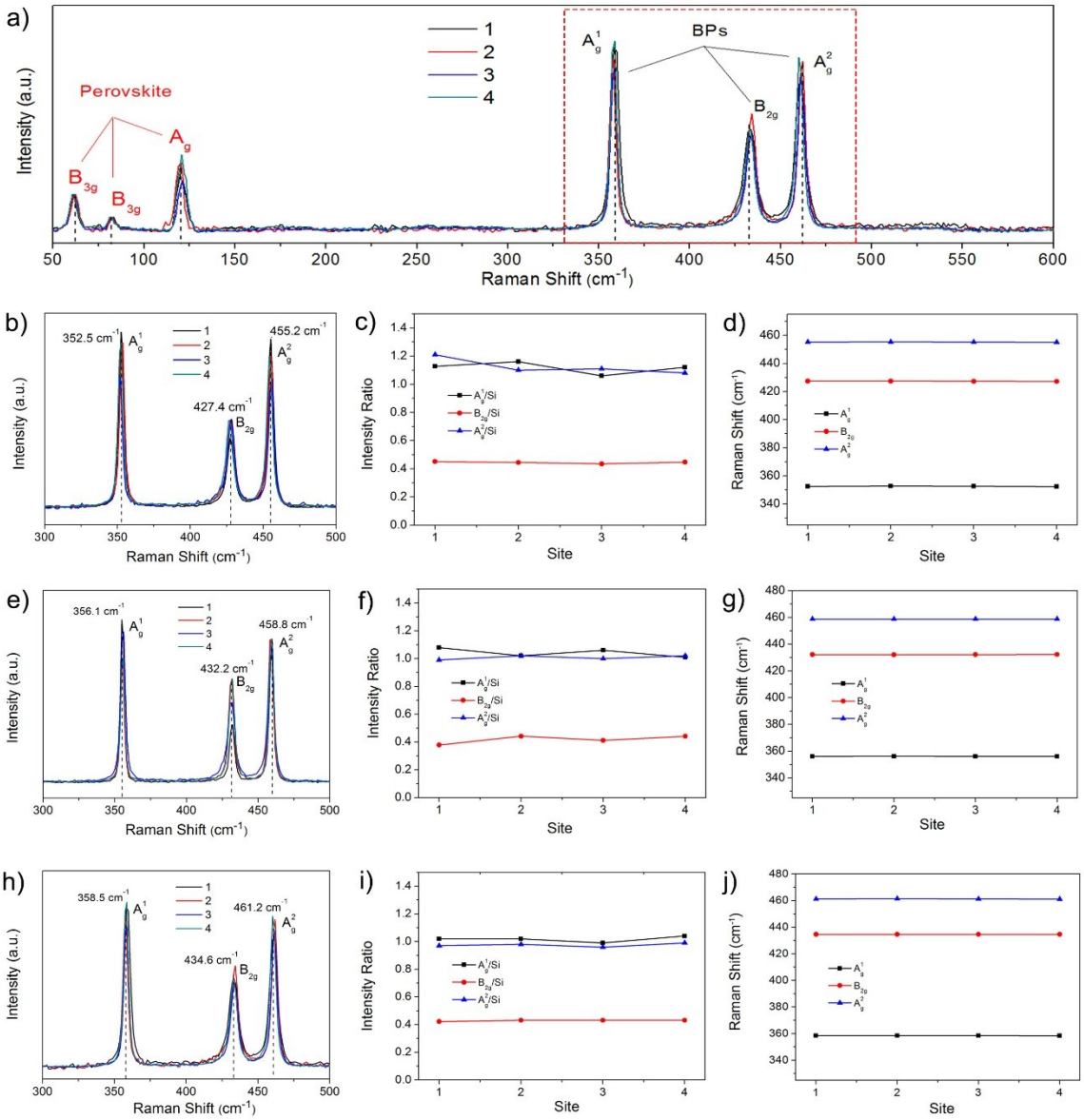

Figure S9 a) Raman spectra of perovskite/BP_{1-2} films in the range from 50 to 600 cm^{-1}. b) Raman spectra of BP_{6-7} film with measured at various sites. c) Raman shift of the three BP_{6-7} modes measured at different sites. d) Raman intensity ratio of BP_{6-7} modes to standard Si mode measured at different sites. e) Raman spectra of BP_{3-4} film with measured at various sites. f) Raman shift of the three BP_{3-4} modes measured at different sites. g) Raman intensity ratio of BP_{3-4} modes to standard Si mode measured at different sites. h) Raman spectra of BP_{1-2} film with measured at various sites. i) Raman shift of the three BP_{1-2} modes measured at different sites. j) Raman intensity ratio of BP_{1-2} modes to standard Si mode measured at different sites.

FigureS9 a shows the Raman spectra of perovskite/BP_{1-2} films in the range from 50 to 600 cm^{-1}. Figure S9 b, e and h represent the Raman spectra of BP_{6-7}, BP_{3-4} and BP_{1-2}, respectively. It is obvious that the Raman peaks shift with layer-number reducing, which are consistent with the Raman spectra in Figure 2a. In addition, the peak positions and peak intensities of four different detected sites are extracted and depicted in Figure S9 c and d (BP_{6-7}), Figure S9 f and g (BP_{3-4}), Figure S9 i and j (BP_{1-2}). The peak positions and intensities in different sites show consistency for each sample, which demonstrates the formation of consistent 1-7 L and the uniform BP film.

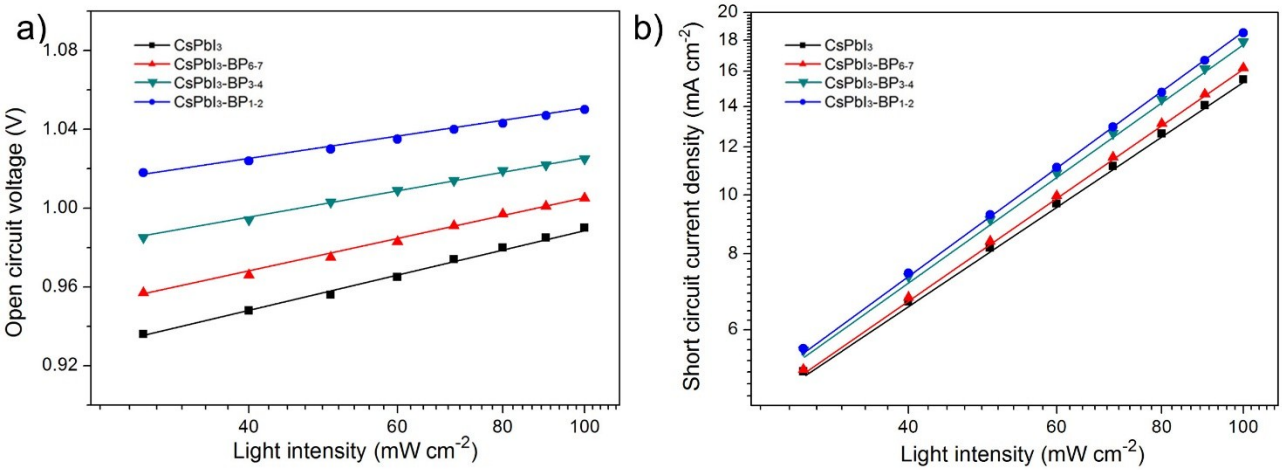

Figure S10 a) J_{sc} and b) V_{oc} as function of light intensity for all-inorganic PSCs based on pristine $CsPbI_3$, $CsPbI_3$-BP_{6-7}, $CsPbI_3$-BP_{3-4} and $CsPbI_3$-BP_{1-2} heterostructures.

To gain more insight into the effect of multi-layer black phosphorous on the recombination in devices, we measured the dependence of J_{sc} and V_{oc} on various light intensities. For these four devices, the V_{oc} increases monotonically with the incident light intensity. According to the equation $V_{oc} = nkT/q \ln(I_{SC}/I_0 + 1)$, the values of the ideality factor are calculated to be 1.74, 1.55, 1.29 and 1.03 for pristine $CsPbI_3$, $CsPbI_3$-BP_{6-7}, $CsPbI_3$-BP_{3-4} and $CsPbI_3$-BP_{1-2}, respectively. In general, the ideality factor derails from unity if Shockley-Read-Hall (SRH) recombination occurs.[S9] In this work, the $CsPbI_3$-BP_{1-2} shows a significant reduction for ideality factor of 1.03, as compared with that of 1.74 for the pristine perovskite device, which demonstrates the trap-assisted SRH recombination is suppressed substantially. Under short-circuit conditions, the current density is followed by the equation of $J_{sc} \propto I^{\alpha}$ ($\alpha \leq 1$). The device with $CsPbI_3$-BP_{1-2} shows slightly increased α value (0.99) closer to unity as compared to 0.92, 0.95 and 0.97 for pristine $CsPbI_3$, $CsPbI_3$-BP_{6-7} and $CsPbI_3$-BP_{3-4}, respectively. This result indicated that almost all free carriers in the device with $CsPbI_3$-BP_{1-2} heterostructure are swept out and collected at the electrodes prior to bimolecular recombination owing to the favorable band alignment and efficient coupling interface.[S10]

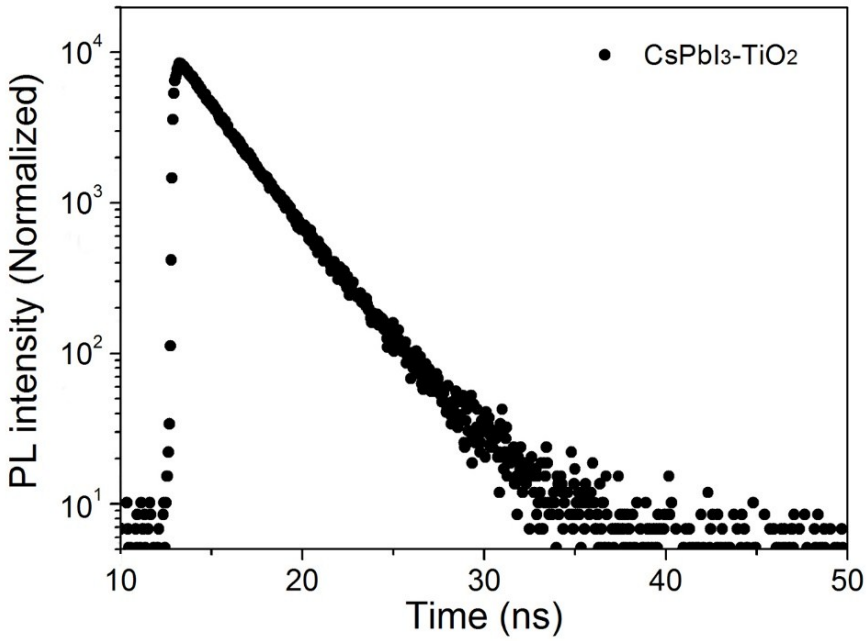

Figure S11 Time-resolved PL spectra of $CsPbI_3$-TiO_2

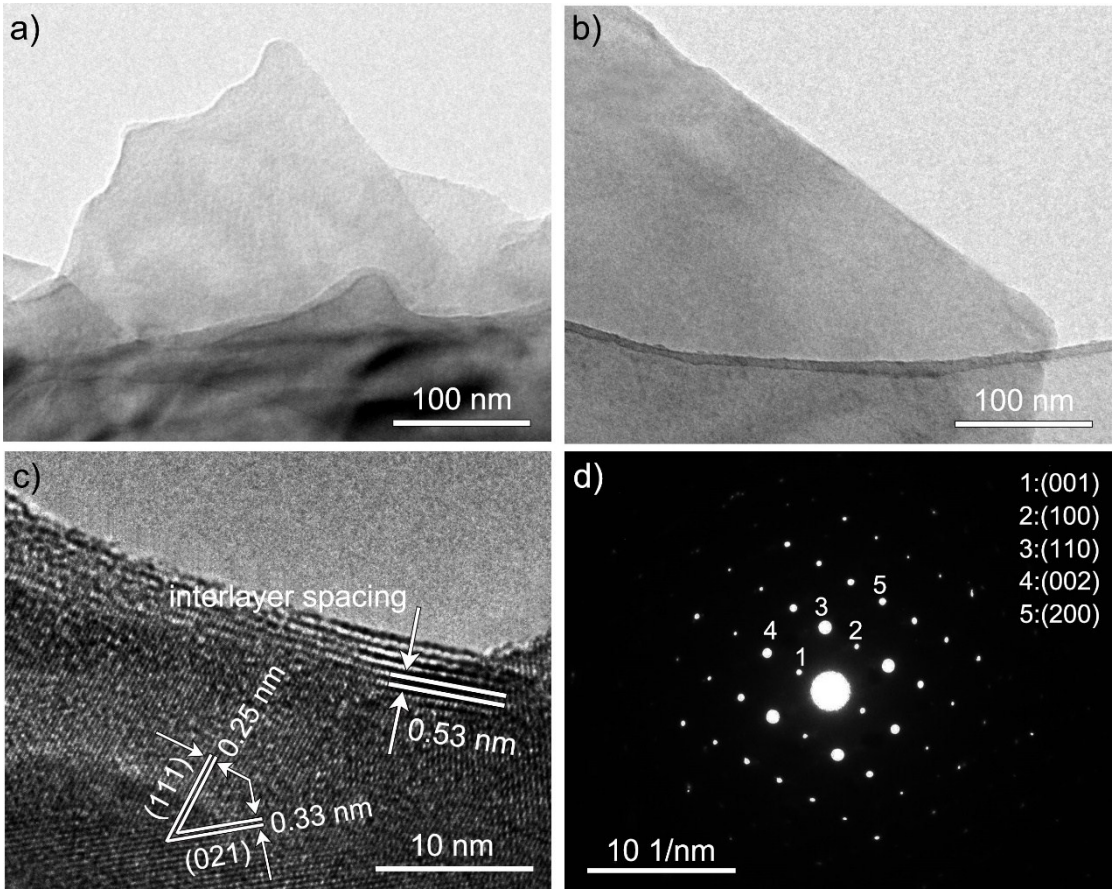

Figure S12 a, b) Low-magnification TEM images of BP nanoflakes. c) High-magnification TEM of BP nanoflakes. d) SAED pattern of BP nanoflakes.

Figure S12 a and b display the low-magnification TEM images of exfoliated BP nanoflakes. The edge of BP nanoflakes show complete structure with defects or fragmentation. As further magnifying the edge of the BP nanoflakes as shown in Figure c of high-magnification TEM image, the BP nanoflake shows a 6-L layer-structure and exhibits uniform and complete edge morphology, demonstrating the high-quality of multi-layer BPs acquired via this technique.

Supplementary Note 1: Optical properties characterization of 2D BPs.

Supplementary Figure 4 shows the UV-vis-NIR spectra of 2D BP film samples with different layer numbers. With the decreasing of layer numbers, the light absorption intensity diminishes in the range from 300 to 600 nm. Moreover, the absorption edges exhibit different gradients. According to the absorption curves, we depict the Tauc plots of BP_{1-2}, BP_{3-4} and BP_{6-7} samples shown in Supplementary Figure 5, which intersect at the 1.2, 1.6 and 1.8 eV, respectively. The light absorption curves of $CsPbI_3$-2D BPs films are presented in Supplementary Figure 6. Compared to pristine $CsPbI_3$, the blending of $CsPbI_3$ and 2D BPs with 50 nm see no obvious increase in absorption intensity, indicating that the improvement to photoresponse via 2D BPs is insignificant.

Supplementary Note 2: Dielectric constant obtained from EIS measurements

From the EIS measurement, the impedance can be divided into two parts including of real and imaginary part as following,

$$Z = Z^{'} + iZ^{''} \tag{S1}$$

Based on the equation (S2), the impedance can be rewritten into capacitance as shown in equation (S3),

$$C = \frac{1}{i\omega Z} \tag{S2}$$

$$C = C^{'} + iC^{''} = \frac{-Z^{''}}{\omega(Z^{'2} + Z^{''2})} + i\frac{-Z^{'}}{\omega(Z^{'2} + Z^{''2})} \tag{S3}$$

By considering the geometrical capacitance (C_g), the dielectric constant can be calculated as following equation,

$$\varepsilon_r = \frac{C_g d}{\varepsilon_0 A} \tag{S4}$$

where ε_0 is the vacuum dielectric constant, d is the perovskite layer thickness of 500 nm, and A is the active area. Via taking the dielectric constant into to account,

$$\varepsilon_r = \varepsilon' + i\varepsilon'' \tag{S5}$$

The real and imaginary part can be derived from,

$$\varepsilon' = \frac{-Z''d}{A\omega\varepsilon_0(Z^{'2} + Z^{''2})} \tag{S6}$$

$$\varepsilon'' = \frac{-Z'd}{A\omega\varepsilon_0(Z^{'2} + Z^{''2})} \tag{S7}$$

Supplementary Note 3: Charge carrier density calculated from Mott-Schottky plots

The charge carrier density of the $CsPbI_3$-2D BPs heterostructures can be calculated from the Mott-Schottky plots according to the equation,

$$\frac{1}{C^2} = \frac{2}{A^2 q \varepsilon \varepsilon_0 N_d}(V_{bi} - V) \quad \text{(S8)}$$

where C is the interfacial capacitance, A the surface area of the semiconductor active interface, V the applied bias potential, q is the elementary charge, N_d the number density of donors, ε and ε_0 represent inorganic perovskite material dielectric constant and vacuum dielectric constant, respectively and V_{bi} is the built-in electric field. Assuming that A corresponds to the electrode area, which was fixed to be 0.09 cm^2 each device sample in our experiment, the charge carrier density obtained from the liner part of the M–S plot for the pristine $CsPbI_3$ device is 1.92×10^{14} cm^{-3}, which is less than the values for $CsPbI_3$-$BP_{6\text{-}7}$ ($2.11\times10^{14}cm^{-3}$), $CsPbI_3$-$BP_{3\text{-}4}$ ($2.55\times10^{14}cm^{-3}$) and $CsPbI_3$-$BP_{1\text{-}2}$ ($2.82\times10^{14}cm^{-3}$) heterostructures.

Supplementary Note 4: The influence of BP layer thickness to carrier extraction efficiency

The PL measurements are conducted based on $CsPbI_3$-2D BP films in order to investigate the effect of BPs layer thickness to carriers excitation efficiency, as well as determine the optimal BP layer thickness. It is evident that with the increase of deposition times, the PL intensity decrease gradually until 15 times, which is corresponded to a thickness of around 50 nm. Further increasing the thickness of BP film shows no obvious decrease in PL intensity. The PL results demonstrate it is most beneficial of a thickness of 50 nm to the carrier extraction due to the maximal PL quenching. Oppositely, further increasing the thickness can cause carrier accumulation in 2D interlayer spacing, and increase the fabrication cost and time.

Supplementary References

S1. Q. Ma, S. Huang, X. Wen, M. A. Green, A. W. Y. Ho-Baollie, *Adv. Energy Mater.* **2016**, *6,* 1502202.

S2. X. Chang, W. Li, L. Zhu, H. Liu, H. Geng, S. Xiang, J. Liu, H. Chen, *ACS Appl. Mater. Interfaces* **2016**, *8*, 33649−33655.

S3. J. Liang, C. Wang, Y. Wang, Z. Xu, Z. Lu, Y. Ma, H. Zhu, Y. Hu, C. Xiao, X. Yi, G. Zhu, H. Lv, Z. Jin, J. Liu, *J. Am. Chem. Soc*. **2016**, *138*, 15829−15832.

S4. J. Duan, Y. Zhao, B. He, Q. Tang, *Angew. Chem. Int. Ed*. **2018**, *57*, 1-6.

S5. S. Xiang, W. Li, Y. Wei, J. Liu, H. Liu, L. Zhu, H. Chen, *Nanoscale*, **2018**, *10*, 9996.

S6. Y. Guo, F. Zhao, J. Tao, J. Jiang, J. Zhang, J. Yang, Z. Hu, J. Chu, *ChemSusChem*, **2019**, *12*, 983 – 989.

S7. J. Liang, Z. Liu, L. Qiu, Z. Hawash, L. Meng, Z. Wu, Y. Jiang, L. Ono, Y. Qi, *Adv. Energy Mater*. **2018**, *8*, 1800504.

S8. K. P. Mubiayi, N. Moloto, M. J. Moloto, *CrystEngComm*, **2018**, *20*, 5275.

S9. D. Bi, W. Tress, M. I. Bar, P. Gao, J. Luo, C. Renevier, K. Schenk, A. Abate, F. Glordano, J. C. Baena, S. M. Zakeeruddin, M. K. Nazeeruddin, M. Gratzel, A. Hagfeldt, Sci. Adv. 2016, 2, 1501170.

S10. D. Credgington, F. C. Jamieson, B. Walker, T.-Q. Nguyen, J. R. Durrant, Adv. Mater. 2012, 24, 2135.